Half-metallicity in a $BiFeO_3/La_{\frac{2}{3}}Sr_{\frac{1}{3}}MnO_3$ superlattice: A first-principles study

Jiwuer Jilili[1], Ulrich Eckern[2] and Udo Schwingenschlögl[1(a)]

[1] *KAUST, PSE Division - Thuwal 23955-6900, Kingdom of Saudi Arabia*
[2] *Institut für Physik, Universität Augsburg - 86135 Augsburg, Germany, EU*

PACS 73.20.-r – Electron states at surfaces and interfaces
PACS 75.70.-i – Magnetic properties of thin films, surfaces, and interfaces
PACS 78.20.-e – Optical properties of bulk materials and thin films

Abstract – We present first-principles results for the electronic, magnetic, and optical properties of the $BiFeO_3/La_{\frac{2}{3}}Sr_{\frac{1}{3}}MnO_3$ heterostructure as obtained by spin-polarized calculations using density functional theory. The electronic states of the heterostructure are compared to those of the bulk compounds. Structural relaxation turns out to have only a minor impact on the chemical bonding, even though the oxygen octahedra in $La_{\frac{2}{3}}Sr_{\frac{1}{3}}MnO_3$ develop some distortions due to the interface strain. While a small charge transfer affects the heterointerfaces, our results demonstrate that the half-metallic character of $La_{\frac{2}{3}}Sr_{\frac{1}{3}}MnO_3$ is fully maintained.

Introduction. – The control of material interfaces at the atomic level has led to novel interfacial properties and functionalities [1]. In material science, multiferroic materials are of interest because they show spontaneous electric and magnetic polarizations. Important examples of single-phase multiferroic materials are $BiFeO_3$ (BFO), $BiMnO_3$, $LuFe_2O_4$, and $BaNiF_4$. Research on room temperature multiferroic materials has focused on $BiFeO_3$ and its derivatives [2] due to the strong electric polarization and potential applications in spintronics and memory devices. However, single-phase multiferroic compounds in general suffer from weak magnetoelectric response [3] and low electrical resistivity [4]. Recently, new strategies for engineering multifunctional multiferroic materials based on composites have been introduced. In comparison to bulk compounds, nanostructured thin films provide more degrees of freedom, such as lattice strain and interlayer interaction, to modify the magnetoelectric behavior. They offer novel ways to investigate the physical mechanisms behind the magnetoelectric effect on the nanoscale [5]. Combining multiferroic and ferromagnetic (FM) materials in a thin-film epitaxial heterostructure provides control of the electron spin polarization through the lattice polarization [6]. Nanoscale composite thin films have been found to be capable of producing relatively large magnetoelectric coefficients [7,8]. From the growth point of view, pulsed-laser deposition [9], molecular beam epitaxy [10] and sol-gel spin-coating [11] have been employed for achieving nanoscale composites.

In recent years the multiferroic FM heterostructure $BFO/La_{1-x}Sr_xMnO_3$ has obtained increasing interest because of its high dielectric constant and excellent ferroelectric behaviour [12]. In addition, a strong magnetoelectric coupling at the interface has been reported in ref. [3]. $BFO/La_{1-x}Sr_xMnO_3$ bilayers reveal a high and homogeneous resistive state for the BFO film that can be used as ferroelectric tunnel barrier [9]. In addition, a significant exchange bias has been observed in this heterostructure [13,14]. The electronic states of bulk BFO and $La_{1-x}Sr_xMnO_3$ have been widely studied experimentally and theoretically. However, research on the heterostructure of these two compounds has been emerging only in recent years, where very few investigations have dealt with *ab initio* calculations using density functional theory. In this work, we therefore study the $BFO/La_{\frac{2}{3}}Sr_{\frac{1}{3}}MnO_3$ (BFO/LSMO) superlattice by first-principles calculations, in particular, to address the interrelation between the interface geometry and the electronic properties.

Computational method. – In order to study the electronic structure and magnetic properties of the BFO/LSMO heterostructure, we apply the full-potential (linearized) augmented plane-wave method, as implemented in the WIEN2k package [15]. This approach is based on density functional theory and is one of the most

(a) E-mail: udo.schwingenschlogl@kaust.edu.sa

Table 1: Structural and technical parameters.

	$BiFeO_3$	$La_{\frac{2}{3}}Sr_{\frac{1}{3}}MnO_3$	$BiFeO_3/La_{\frac{2}{3}}Sr_{\frac{1}{3}}MnO_3$
Property	AFM insulator	FM half-metal	
Structure	hexagonal	hexagonal	hexagonal
Lattice parameters	$a=b=5.57$ Å $c=13.86$ Å $\alpha=\beta=90°$, $\gamma=120°$	$a=b=5.49$ Å $c=13.37$ Å $\alpha=\beta=90°$, $\gamma=120°$	$a=b=5.54$ Å $c=27.24$ Å $\alpha=\beta=90°$, $\gamma=120°$
Space group	R3c	$R\bar{3}c$	P3
Atoms	30 (6 BFO)	30 (6 LSMO)	60
Inequivalent atoms	18	6	36
Method	GGA + U (AFM)	GGA + U (FM)	GGA + U
Onsite interaction	$U=7$ eV $=0.52$ Ry $J=0$ eV	$U=5$ eV $=0.37$ Ry $J=0$ eV	$U=7$ eV $=0.52$ Ry (Fe) $U=5$ eV $=0.37$ Ry (Mn)

accurate schemes of solid-state electronic-structure calculations [16]. The generalized-gradient approximation with onsite Coulomb interaction and self-interaction correction (GGA + U) is used for the exchange-correlation functional [17–19]. The Coulomb interaction parameter U and exchange parameter J are introduced to account for the onsite electron-electron interaction in the localized $3d$ orbitals of the transition metals. We set $U=5$ eV for Mn, $U=7$ eV for Fe, and $J=0$ eV for both Fe and Mn, based on previous electronic structural calculations of bulk BFO [20,21] and LSMO [22].

Brillouin zone integrations are performed on a $6\times6\times2$ Monkhorst-Pack k-mesh [23] with 16 points in the irreducible wedge of the Brillouin zone. We have tested different meshes for BFO and LSMO to confirm that this mesh is sufficiently fine to guarantee converged results. The muffin-tin radii are set to 1.5, 1.95, 2.13, and 2.48 Bohr radii for O, Fe, Bi, and Sr, respectively, and to 1.93 for both La and Mn. Moreover, an energy cutoff given by $R_{mt}K_{max}=7$ with $\ell_{max}=10$ is employed. Self-consistency is achieved with an energy convergence of 10^{-3} Ry. In our calculations, the charge densities are represented by 24535, 6414, and 47521 plane waves for BFO, LSMO, and BFO/LSMO, respectively. Full relativistic effects are taken into account for the core states, while the scalar relativistic approximation is used for the valence states. The basis set consists of O $2s^2$ $2p^4$, Mn $3s^2$ $3p^6$ $3d^5$ $4s^2$, Fe $3s^2$ $3p^6$ $3d^6$ $4s^2$, Sr $4s^2$ $4p^6$ $5s^2$, La $4d^{10}$ $5s^2$ $6s^2$ $5p^6$ $5d^1$, and Bi $5p^6$ $5d^{10}$ $6s^2$ $6p^3$ orbitals. In order to address the effect of the structural relaxation at the interfaces in the BFO/LSMO superlattice on the physical properties, the atomic positions are fully relaxed with a force tolerance of 2 mRy/Bohr. Moreover, the density of states (DOS) is calculated with a Gaussian broadening of 5 mRy. A summary of the employed structural and technical parameters is given in table 1.

Results and discussion. – Bulk BFO and LSMO have a rhombohedrally distorted perovskite structures

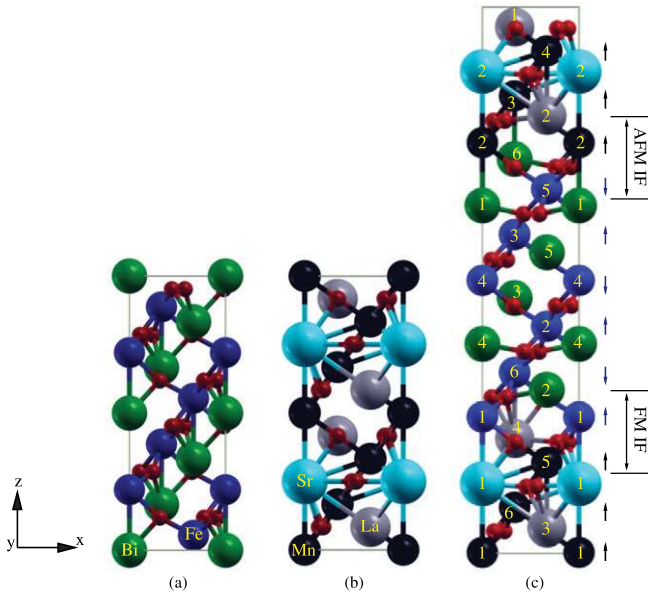

Fig. 1: (Colour on-line) Structure of bulk $BiFeO_3$, bulk $La_{\frac{2}{3}}Sr_{\frac{1}{3}}MnO_3$, and the BFO/LSMO superlattice. Small red spheres denote O atoms, while the other atoms are indicated in the figure. Arrows indicate the orientation of the magnetic moments, and AFM IF and FM IF denote, respectively, the locations of the antiferromagnetic and the ferromagnetic interface.

with hexagonal lattice parameters $a=5.58$ Å, $c=13.87$ Å [24] and $a=5.49$ Å, $c=13.37$ Å [25], respectively, as shown in figs. 1(a) and (b). Moreover, BFO exhibits a ferroelectric transition at $T_C=1100$ K (from ferroelectricity to paraelectricity) and a magnetic transition at $T_N=643$ K [26] (from an antiferromagnet to a paramagnet). The antiferromagnetic (AFM) order in BFO is of G-type [27]. Hole-doped $La_{\frac{2}{3}}Sr_{\frac{1}{3}}MnO_3$ is a double-exchange ferromagnet with metallic conductivity below $T_C=370$ K [28]. Starting from the bulk materials, we set up a hexagonal supercell by stacking the bulk

unit cells along the $[001]_{\rm hex}$ direction, see fig. 1(c), which shows two BFO unit cells in the center sandwiched between LSMO unit cells. Due to the periodic boundary conditions, we therefore have alternating BFO and LSMO layers of two unit cell thickness. Our supercell contains 36 inequivalent atomic sites and 60 atoms in total. The lattice constants parallel to the interfaces are chosen to assume the average value $a = b = 5.54\,$Å, while the perpendicular length is $c = 27.24\,$Å, *i.e.*, the sum of the underlying BFO and LSMO bulk lattice constants. By construction, our supercell contains two interfaces, one FM and the other AFM, because BFO is subject to AFM order and LSMO to FM order. Thus, the Fe atoms at the two interfaces have the magnetic moments oriented in opposite direction and the coupling between BFO and LSMO is FM at one interface and AFM at the other one.

After the structural relaxation of the BFO/LSMO superlattice we find a significant modification of the structure in the LSMO region, specifically, the distortion of the MnO_6 octahedra is extended to the BFO. In other words, the bond angles within the MnO_6 octahedra change such that they resemble the FeO_6 octahedra. For a deeper analysis, we compare the structure of our superlattice with the corresponding structural data of the bulk compounds. The O-Mn-O (Mn-O-Mn) bond angles decrease by up to 6° (10°) from their bulk value of 180° (173°). This alteration indicates that the O octahedra in our superlattice no longer maintain the almost perfect octahedral shape as found in bulk LSMO. The Mn-O bond length (1.94 Å in the bulk) at the AFM interface increases to 2.04 Å, whereas the Fe-O bond length (2.11 Å in the bulk) at the FM interface shrinks to 2.07 Å. These alterations are either due to the strain induced by the lattice mismatch or the broken translational symmetry at the interface. Importantly, the off-centering of the Fe atoms within the O octahedra shows significant modifications in the superlattice. While in bulk BFO there are three Fe-O bond lengths of 1.96 Å and three other of 2.11 Å, these values change to 2.00 Å and 2.03 Å, respectively, except for the FM interface, see above. This fact implies that the ferroelectric behavior is reduced due to the proximity of the LSMO. We note that this finding does not contradict the experimental situation of ref. [12], because in that work the film thickness is much higher. We will discuss below how the structural distortions in the superlattice affect the orbital occupations and spin polarization at the two interfaces.

The total DOS is presented in fig. 2 for bulk BFO (top left) and bulk LSMO (top right). The BFO DOS shows that in the low-energy range between about −8 eV and −7 eV the Fe 3*d* states dominate. On the other hand, the region from −6 eV to the Fermi energy (E_F) is mainly due to the Bi 4*p* and O 2*p* states. There is a strong hybridization between Bi and O, which plays an important role for the ferroelectricity, because in BFO ferroelectricity results from the local distortion introduced by the stereochemically active $6s^2$ lone pair of electrons of the Bi^{3+}

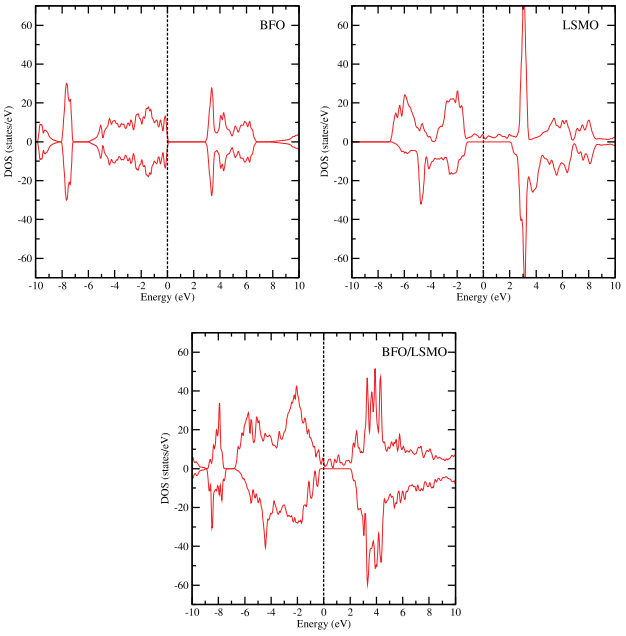

Fig. 2: (Colour on-line) Total DOS of bulk BFO, bulk LSMO, and the BFO/LSMO superlattice.

cation [29]. From 3 eV to 6.8 eV (the conduction band), the Fe 3*d* and Bi 4*p* states are dominant with small contributions from the O 2*p* states. We find that the Fe 3*d* states at the conduction band minimum are hybridized with O 2*p* states to some extent.

In general, BFO displays an insulating character with a band gap of 2.8 eV, which is determined by the energetical seperation between strongly hybridized O 2*p* and Fe 3*d* valence states and the bottom of the conduction band. The calculated band gap is in reasonable agreement with the experimental results of 2.5 eV [30] and 2.7 eV [31]. In the LSMO DOS the majority spin metallicity results from the broad Mn 3*d* and O 2*p* hybridized states in the energy range from −7.2 eV to 2.6 eV, while E_F is located in the minority spin band gap. The shape of the valence DOS with two broad peaks agrees well with results from X-ray photoemission spectroscopy [32]. Sharp peaks at 3.3 eV (3.8 eV) are mainly due to La *f* (Mn *d*) contributions. From about 6.5 eV to 8.3 eV the Sr *d* states are dominant. The LSMO DOS exhibits a half-metallic character with a spin minority band gap of 3.2 eV. This value is larger than reported in previous studies, mainly because we use a higher Coulomb parameter of $U = 5\,$eV. In fact, the GGA+U approach with this U value produces an increased band gap and a more consistent picture of the electronic structure for the two bulk compounds.

Importantly, the total DOS of the superlattice in fig. 2 (bottom) clearly shows a half-metallic character with a minority spin band gap of 2.2 eV. This fact indicates that our superlattice preserves the half-metallic nature of bulk LSMO. We note that the Fe *d*, Sr *d*, La *f*, and Bi *p* states do not contribute to the metallicity in the spin majority channel. Although the Fe 3*d* states at the

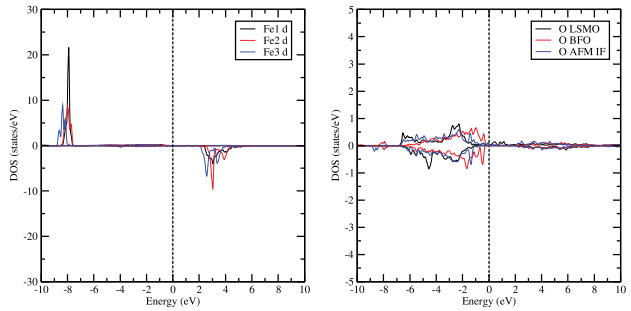

Fig. 3: (Colour on-line) Partial DOS of Fe (left) and O (right) in the BFO/LSMO superlattice.

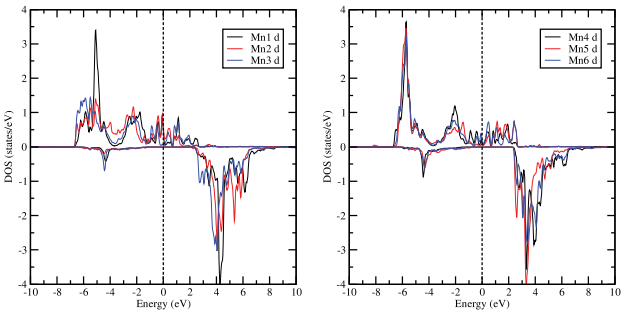

Fig. 4: (Colour on-line) Partial DOS of Mn in the BFO/LSMO superlattice.

conduction band minimum are slightly shifted to lower energy in the BFO/LSMO superlattice with respect to the bulk Fe states, due to differences in the electrostatic background, they are still far from E_F and therefore do not contribute to the metallicity. The energetical shift implies that there is a transfer of charge in the superlattice, which mainly affects the states between $-2\,\mathrm{eV}$ and $2\,\mathrm{eV}$. In the vicinity of E_F the DOS predominately can be traced back to hybridized Mn $3d$ and O $2p$ states. The band gap in the minority channel is reduced with respect to bulk LSMO because bulk BFO O $2p$ minority states appear between $-1\,\mathrm{eV}$ and $0\,\mathrm{eV}$. Strain effects, which also could modify the band gap, seem to play a subordinate role.

To distinguish the atoms near and far from the interface, we label the atoms as shown in fig. 1(c). The Fe d (left) and O p (right) DOSs are addressed in fig. 3. The sites Fe1 and Fe6 are located near the FM interface, the sites Fe3 and Fe5 near the AFM interface, and the sites Fe2 and Fe4 close to the center of the BFO region. These pairs of atoms therefore exhibit similar DOS curves but with opposite spins. We observe that Fe3 (located near the AFM interface) appears at lower energy than Fe1 (located near the FM interface), where Fe2 (located in a bulk-like environment) resembles the bulk DOS. A similar behavior is found for Sr, La, and Bi. In general, a more positive electrostatic background will lead to electronic states at lower energy. According to the above analysis, the FM interface thus is characterized by a less positive electrostatic background. As a consequence, we should obtain less charge near the FM interface, while the more positive electrostatic background near the AFM interface should lead to higher orbital occupations. We will discuss this point in the next section. Finally fig. 3 (right) shows the DOS for three selected O atoms from the LSMO region, the BFO region, and the AFM interface. We find that only O atoms in the LSMO region contribute to the metallicity of the BFO/LSMO superlattice, while the O atoms in the BFO region give essentially no contribution except for those located exactly at the AFM interface. Strong hybridization between the Mn and O states near E_F is reflected by common peaks in the Mn and O DOS.

In fig. 4 we display the partial Mn $3d$ DOS. The main contribution to the DOS at E_F and thus to the metallicity

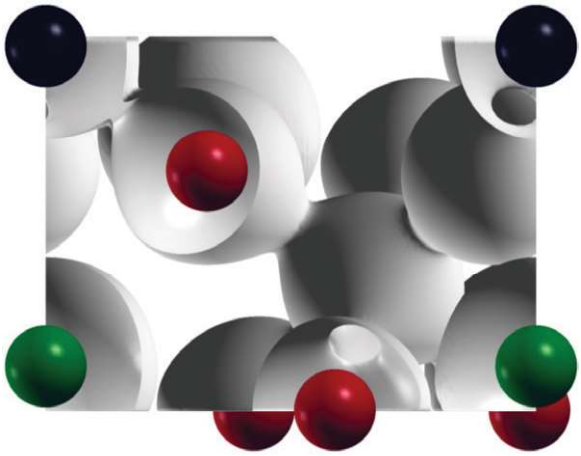

Fig. 5: (Colour on-line) Valence charge density in the vicinity of the AFM interface, using the projection of fig. 1.

is due to the spin majority Mn $3d$ states. The sites Mn2 and Mn3 (located near the AFM interface), Mn5 and Mn6 (located near the FM interface), and Mn1 and Mn4 (located in a bulk-like environment) exhibit a similar DOS; also the differences between these groups are not significant. Finally, we show in fig. 5 the calculated valence charge density near the AFM interface in order to demonstrate the bonding within the Fe-O-Mn network. The same projection and colors as in fig. 1(c) are employed.

We first address the orbital occupations in our superlattice. As to be expected, the Bi and Mn atoms lose some charge, specifically atom Mn2 (Mn5) near the AFM (FM) interface loses 0.02 (0.07) electrons. Atom Bi6 (Bi2) near the AFM (FM) interface loses 0.01 (0.02) electrons. On the other hand, each La atom in the superlattice gains 0.02 electrons, while Sr2 near the AFM interface gains 0.02 electrons and Sr1 near the FM interface gains 0.03 electrons. Charge differences turn out to be negligible for the Fe atoms, except for Fe5 near the AFM interface which gains 0.01 electrons. All O atoms lose some charge (< 0.02 electrons) except for those at the FM interface. Comparing the atomic charges near the two interfaces, we find a bit less charge at the FM interface than at the AFM interface, which agrees with the above analysis of the DOS and

implies that the orbital reconstruction at the AFM interface is larger than at the FM interface.

So far we have investigated the change of the orbital occupations in the BFO/LSMO superlattice with respect to the bulk compounds. However, such changes have implications for the magnetic moments. The average Mn magnetic moment in the superlattice is found to be $3.54\,\mu_B$, which is slightly larger than the bulk value of $3.52\,\mu_B$, in reasonable agreement with the experimentally reported value of $3.67\,\mu_B$/Mn [33]. Interestingly, the Mn magnetic moment varies significantly near the interface to the BFO, which supports magnetoelectric coupling. In agreement with the DOS in fig. 4, Mn2 (Mn5) gains (loses) a magnetic moment of 0.33 (0.38) μ_B. The Mn magnetic moments are determined by the majority spin electrons while the minority spin contributions are negligible around E_F. The reduction of the magnetic moment near the FM interface thus is due to the loss of majority spin states.

The magnetic moments of all the Fe atoms almost keep their bulk values, except for the slight decrease of $0.02\,\mu_B$ for Fe1 near the FM interface. The average Fe magnetic moment is $4.2\,\mu_B$, which is similar to the reported value of a previous GGA+U calculation using the same U parameter [21]. However, this value is slightly larger than the experimental magnetic moment of 3.7 μ_B [34]. This observation confirms that the GGA+U method slightly overestimates Fe magnetic moments [35]. According to the reported variations of the magnetic moment between the bulk and the superlattice, it can be concluded that the FM interface is subject to a reduced spin polarization, whereas the spin polarization is enhanced at the AFM interface. As a consequence, an AFM spin order across the interface is energetically favourable as compared to a FM spin order, in agreement with the findings reported in ref. [36]. Yu and coworkers [37] also suggested that the coupling between the Mn bulk and Fe interfacial spins is antiparallel according to the opposite signs observed in Mn and Fe X-ray magnetic circular dichroism.

In general, interaction between O atoms and magnetic ions plays an important role for the magnetic properties of transition metal oxides. For BFO, O vacancies have been found to result in a noticeable modification of the magnetism due to a transition of the Fe oxidation state from 3+ to 2+ [38]. Both experimentally and theoretically it has been suggested that O vacancies enhance the ferromagnetism because they alter the distance between the Fe ions and, therefore, the strength of the Dzyaloshinskii-Moriya interaction [39]. Similar effects can be expected for the BFO/LSMO superlattice.

We next address the optical properties of the BFO/LSMO superlattice, in particular the imaginary part of the dielectric function, Im(ϵ), and the reflectivity, $R(\omega)$. Figure 6 compares results for the superlattice to those of bulk BFO and LSMO, separately for the majority and minority spins. Since BFO is not subject to spin polarization, the two spin channels are degenerate in this case. The results clearly reflect that bulk BFO is

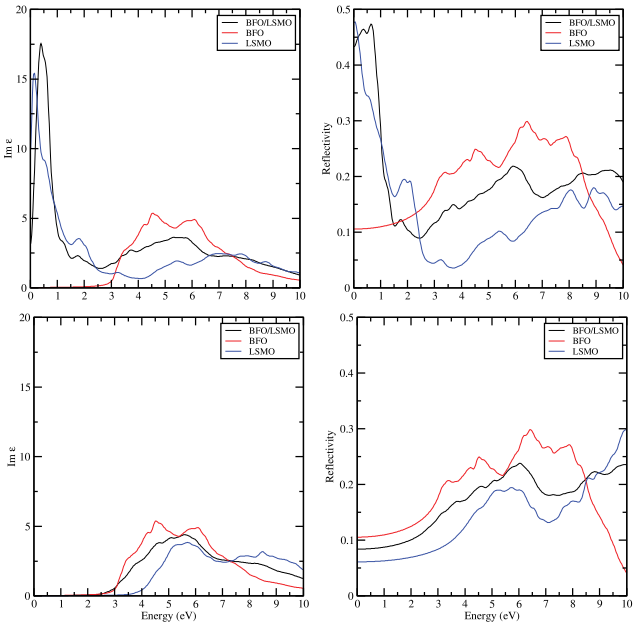

Fig. 6: (Colour on-line) Imaginary part of the dielectric function (xx component) and reflectivity of the BFO/LSMO superlattice. Top: majority spins, bottom: minority spins. While the xx and yy components of the dielectric function are obviously identical, we find that also the zz component is very similar.

insulating with an optical band gap of about 2.5 eV. There appear mainly two peaks in $R(\omega)$, with some additional subpeaks. The peak around 4 eV reflects transitions of O p electrons into unoccupied Fe d states, whereas the peak around 6 eV corresponds to transitions of O p electrons into the Bi p conduction bands. These findings match well with previous first-principles calculations reported in ref. [40]. Our results for Im(ϵ) agree much better with the experimental situation [31] than the data obtained in ref. [20], in particular, for the 4 eV peak, for which even the substructure reproduces the experimental spectrum. The better agreement is probably due to the different onsite interaction parameter applied in our study.

Bulk LSMO shows a high reflectivity in the low-energy range for the majority spin states, the metallic Drude peak. For the minority spin states, both $R(\omega)$ and Im(ϵ) exhibit a band gap, reflecting the half-metallic character of LSMO. The spin majority reflectivity peak at 2 eV is consistent with the experimental peak with respect to energy and magnitude [41,42]. It is due to transitions from the hybridized O p and Mn d states into the Mn d states in the conduction band. At 3.3 eV we observe the remainder of the dipole forbidden transition from the O p into the La f states. Concerning the minority spin channel, the pronounced $R(\omega)$ peak between 5 and 6 eV is due to transitions of O p electrons into Mn d conduction states. Previous calculations on the optical properties of LSMO [43] have suggested transitions from Mn d t_{2g} into Mn d e_g states in the majority spin channel, and from O $2p$ into Mn d t_{2g} and e_g states in the minority spin channel.

We find that the BFO/LSMO superlattice also shows a high reflectivity in the low-energy range for the majority spin states, and a band gap for the minority spin states, thus merging the individual properties of bulk BFO and LSMO. The half-metallic behavior discussed before for the DOS accordingly is reflected by the optical spectrum. For the minority spin channel, $\mathrm{Im}(\epsilon)$ shows that the absorption begins above 2 eV for the superlattice, whereas for bulk LSMO absorption occurs only above 3 eV. The required excitation energy thus is reduced, since the half-metallic band gap is smaller in the case of the superlattice. The calculated optical band gaps match well with the minority spin band gaps in the DOS, which amount to 2.2 and 3.2 eV in the case of the BFO/LSMO superlattice and bulk LSMO, respectively. We note that a reduced minority spin band gap opens potential applications in spintronic devices and photocatalyst materials. As compared to the bulk compounds, we observe shifts in the energetical positions of the $R(\omega)$ peaks. In the energy range from 3 to 6 eV we notice a shift towards lower energy, and above 8 eV a shift towards higher energy. This behavior corresponds to the aforementioned modifications of the DOS, in particular, the shift of states of atoms near the AFM (FM) interface to lower (higher) enery. In general, the optical spectrum of the BFO/LSMO superlattice is well understood in terms of merged bulk BFO and LSMO spectra. A clear optical anisotropy is found neither for the two bulk compounds nor for the superlattice.

Conclusion. – We have investigated the structural, magnetic, and optical properties of hexagonal (rhombohedral) BFO, LSMO, and a BFO/LSMO superlattice using the GGA+U approach. As concerns the structural properties, our calculations are in good qualitative and quantitative agreement with the experimental situation. In addition, they reproduce the insulating and half-metallic natures of bulk BFO and LSMO, respectively. The Fe magnetic moments are found to slightly exceed the experimental values, which is a well-known phenomenon for GGA + U calculations. On the other hand, the calculated band gap agrees well with experiment. Intriguingly, the BFO/LSMO superlattice maintains the half-metallic character of bulk LSMO. Structural relaxation and charge transfer are present at both interfaces, but are not strong enough to significantly modify the bulk properties.

* * *

Financial support by the Deutsche Forschungsgemeinschaft (TRR 80) is gratefully acknowledged.

REFERENCES

[1] Yu P. *et al.*, *Proc. Natl. Acad. Sci. U.S.A.*, **109** (2012) 9710.
[2] Eerenstein W., Mathur N. D. and Scott J. F., *Nature*, **442** (2006) 759.
[3] Calderon M. J. *et al.*, *Phys. Rev. B*, **84** (2011) 024422.
[4] Higuchi T. *et al.*, *Phys. Rev. B*, **78** (2008) 085106.
[5] Nan C. *et al.*, *J. Appl. Phys.*, **103** (2008) 031101.
[6] Krishnan P. S. S. R. *et al.*, *J. Appl. Phys.*, **109** (2011) 034103.
[7] Naik V. B. and Mahendiran R., *Solid State Commun.*, **149** (2009) 754.
[8] Yan L. *et al.*, *J. Appl. Phys.*, **107** (2010) 064106.
[9] Béa H. *et al.*, *Appl. Phys. Lett.*, **88** (2006) 062502.
[10] Luo B. C. *et al.*, *Chin. Phys. Lett.*, **29** (2012) 18104.
[11] Zhou C. C. *et al.*, *Solid. State Commun.*, **150** (2010) 1334.
[12] Ke Q. Q. *et al.*, *J. Electrochem. Soc.*, **159** (2012) G11.
[13] Wu S. M. *et al.*, *Nat. Mater.*, **9** (2010) 756.
[14] Yu P. *et al.*, *Phys. Rev. Lett.*, **105** (2010) 027201.
[15] Blaha P. *et al.*, *WIEN2k* (TU Vienna, Vienna) 2001.
[16] Schwarz K., Blaha P. and Madsen G. K. H., *Comput. Phys. Commun.*, **147** (2002) 71.
[17] Anisimov V. I., Zaanen J. and Andersen O. K., *Phys. Rev. B*, **44** (1991) 943.
[18] Perdew J. P., Burke K. and Ernzerhof M., *Phys. Rev. Lett.*, **77** (1996) 3865.
[19] Svane A., *Phys. Rev. Lett.*, **72** (1994) 1248.
[20] Ju S., Cai T. Y. and Guo G. Y., *J. Chem. Phys.*, **130** (2009) 214708.
[21] Bi L. *et al.*, *Phys. Rev. B*, **78** (2008) 104106.
[22] Colizzi G., Filippetti A. and Fiorentini V., *Phys. Rev. B*, **76** (2007) 064428.
[23] Monkhorst H. J. and Pack J. D., *Phys. Rev. B*, **13** (2007) 5188.
[24] Selbach S. M. *et al.*, *Adv. Mater.*, **20** (2008) 3692.
[25] Venkataiah G., Prasad V. and Reddy P. V., *J. Alloys Compd.*, **429** (2007) 1.
[26] Smolenski G. A. and Chupis I. E., *Sov. Phys. Usp.*, **25** (1982) 475.
[27] Kiselev S. V., Ozerov R. P. and Zhdanov G. S., *Sov. Phys. Dokl.*, **7** (1963) 742.
[28] Krempaský J. *et al.*, *Phys. Rev. B*, **77** (2008) 165120.
[29] Baettig P., Ederer C. and Spaldin N. A., *Phys. Rev. B*, **72** (2005) 214105.
[30] Gao F. *et al.*, *Appl. Phys. Lett.*, **89** (2006) 102506.
[31] Ihlefeld J. F. *et al.*, *Appl. Phys. Lett.*, **92** (2008) 142908.
[32] Offi F. *et al.*, *Phys. Rev. B*, **77** (2008) 174422.
[33] Lu H. *et al.*, *Appl. Phys. Lett.*, **100** (2012) 232904.
[34] Sosnowska I. *et al.*, *J. Magn. & Magn. Mater.*, **160** (1996) 384.
[35] Wang Y. *et al.*, *Acta Mater.*, **59** (2011) 4229.
[36] Neumann R. F., Bahiana M. and Binggeli N., *EPL*, **100** (2012) 67002.
[37] Yu P., Chu Y. H. and Ramesh R., *Mater. Today*, **15** (2012) 320.
[38] Ederer C. and Spaldin N. A., *Phys. Rev. B*, **71** (2005) 224103.
[39] Fang L. *et al.*, *Appl. Phys. Lett.*, **97** (2010) 242501.
[40] Liu K. *et al.*, *J. Alloys Compd.*, **509** (2011) 1901.
[41] Okimoto Y. *et al.*, *Phys. Rev. B*, **55** (1997) 4206.
[42] Mechin L. *et al.*, *J. Appl. Phys.*, **98** (2005) 103902.
[43] Liu H. L. *et al.*, *J. Appl. Phys.*, **99** (2006) 043908.